



ELSEVIER

Available online at www.sciencedirect.com**ScienceDirect**journal homepage: www.elsevier.com/locate/he**Review Article****Overview of hydrogen embrittlement in high-Mn steels**

Motomichi Koyama ^{a,*}, Eiji Akiyama ^b, Young-Kook Lee ^c, Dierk Raabe ^d,
Kaneaki Tsuzaki ^{a,e}

^a Department of Mechanical Engineering, Kyushu University, Motooka 744, Nishi-ku, Fukuoka, Fukuoka, Japan

^b Institute for Materials Research, Tohoku University, Katahira 2-1-1, Aoba-ku, Sendai, 980-8577, Japan

^c Department of Materials Science and Engineering, Yonsei University, Seoul, 120-749, Republic of Korea

^d Max-Planck-Institut für Eisenforschung GmbH, Max-Planck-Straße 1, 40237, Düsseldorf, Germany

^e HYDROGENIUS, Kyushu University, Motooka 744, Nishi-ku, Fukuoka, Fukuoka, Japan



CrossMark

ARTICLE INFO**Article history:**

Received 30 January 2017

Received in revised form

22 February 2017

Accepted 28 February 2017

Available online 21 March 2017

Keywords:

Hydrogen embrittlement

Austenitic steel

Martensitic transformation

Deformation twinning

Hydrogen segregation

ABSTRACT

Hydrogen and fuels derived from it will serve as the energy carriers of the future. The associated rapidly growing demand for hydrogen energy-related infrastructure materials has stimulated multiple engineering and scientific studies on the hydrogen embrittlement resistance of various groups of high performance alloys. Among these, high-Mn steels have received special attention owing to their excellent strength – ductility – cost relationship. However, hydrogen-induced delayed fracture has been reported to occur in deep-drawn cup specimens of some of these alloys. Driven by this challenge we present here an overview of the hydrogen embrittlement research carried out on high-Mn steels. The hydrogen embrittlement susceptibility of high-Mn steels is particularly sensitive to their chemical composition since the various alloying elements simultaneously affect the material's stacking fault energy, phase stability, hydrogen uptake behavior, surface oxide scales and interstitial diffusivity, all of which affect the hydrogen embrittlement susceptibility. Here, we discuss the contribution of each of these factors to the hydrogen embrittlement susceptibility of these steels and discuss pathways how certain embrittlement mechanisms can be hampered or even inhibited. Examples of positive effects of hydrogen on the tensile ductility are also introduced.

© 2017 Hydrogen Energy Publications LLC. Published by Elsevier Ltd. All rights reserved.

Contents

Introduction	12707
Microstructure effects assisting crack formation	12707
Importance of Σ_3 twin boundary: coherency and segregation	12710
Strain rate dependence: Kinetic Effects associated with hydrogen and carbon	12712

* Corresponding author.

E-mail address: koyama@mech.kyushu-u.ac.jp (M. Koyama).

<http://dx.doi.org/10.1016/j.ijhydene.2017.02.214>

0360-3199/© 2017 Hydrogen Energy Publications LLC. Published by Elsevier Ltd. All rights reserved.

Effects of Al on hydrogen uptake and embrittlement behavior	12713
Effects of alloying elements Mn, Si, Cu, and P in high-Mn steels	12716
Embrittlement behavior in hydrogen gas atmospheres	12717
Ways to enhance hydrogen degradation resistance	12718
Summary	12719
Acknowledgements	12719
References	12719

Introduction

Since the development of Hadfield steel in 1882 [1], high-Mn steels have been recognized to have superior work hardening capacity enabling excellent ductility-strength balance. In particular, the development of twinning-induced plasticity (TWIP) steels, which constitute a class of austenitic alloys characterized by deformation driven twin and – in some cases – martensite formation, created renewed interest in high-Mn steels as candidate materials for manufacturing structural parts for automobiles [2–6]. Moreover, high-Mn steels and compositionally more complex yet related alloys with new functions have been developed, e.g., seismic-resistant alloys [7–9], biodegradable alloys [10–12], and high entropy alloys [13–15]. With this background, various high-Mn steels have been investigated regarding their mechanical response under severe loading conditions and harsh environments such as for instance high speed deformation [16,17], cryogenic temperatures [18,19], and hydrogen atmospheres.

Currently, many countries are undertaking efforts towards developing a hydrogen-based energy supply and consumption chain which is capable of matching the needs of modern mobile and industrialized societies. In this regard, the development of hydrogen-resistant steels as well as hydrogen-containing materials has become a bottleneck technology required for the cost-efficient realization of hydrogen-energy-related generation, storage and processing infrastructures.

From a viewpoint of mechanical properties when exposed to hydrogen charging environments, the low diffusivity of hydrogen in fcc austenite high-Mn steels, which suppresses severe dislocation/hydrogen interactions, had been projected to enable the development of a new class of hydrogen-resistant structural materials. For instance, TWIP steels indeed have higher resistance to hydrogen embrittlement when compared to low carbon steels, martensitic steels, dual-phase steels, and transformation-induced plasticity steels [20–22]. However, high-Mn steels may also undergo hydrogen-related fracture in some cases where both, severe mechanical and hydrogen charging conditions apply, such as occurring when the materials are subjected to a high current density [23,24] and to heavy deformation as deep-drawing [25–28]. An example of hydrogen-induced delayed fracture in high-Mn austenitic steels is shown in Fig. 1. Towards the improvement of hydrogen embrittlement susceptibility of high-Mn steels with high strength, it is thus inevitable to better understand the underlying factors and mechanisms affecting the material's resistance to hydrogen embrittlement.

A specific key strategy for enhancing the resistance of high Mn steels to hydrogen embrittlement lies in controlling the

thermodynamic stability of the austenite phase through the addition of Mn [29,30]. Slow strain rate tensile tests (SSRT) were conducted using hydrogen-charged specimens of austenitic Fe-high Mn-C steels [24,31,32] for the quantitative evaluation of the material's hydrogen embrittlement susceptibility. The SSRT results demonstrated reduction in tensile ductility and various modes of hydrogen-assisted cracking. Later on similar coupled compositional – mechanical studies revealed that the vulnerability of the alloys to hydrogen-induced delayed cracking can be improved by the addition of Al in solid solution [25,32,33].

Despite numerous attempts to understand all the underlying internal damage effect, the mechanism of hydrogen embrittlement in high-Mn steels has not yet been elucidated, probably due to the many interacting influence factors. In general, hydrogen embrittlement susceptibility of a given material depends on the strength level [34,35], residual stress [25,36], hydrogen content [37,38], and microstructural features such as lattice defect density [39,40]. Moreover, similar to the case of Fe-Cr-Ni austenitic stainless steels [41,42], the formation of α' -martensite is a critical factor causing hydrogen embrittlement in high-Mn austenitic steels. In addition, ϵ -martensite formation, deformation twinning, strain aging, formation of surface oxidation layers, etc. seem to affect the material's hydrogen embrittlement susceptibility. In order to explore the individual effects associated with these factors in detail, several investigations with more systematic composition and microstructure control as well as pertinent simplifications of the embrittlement boundary conditions have been presented in the past [32,43–45].

This review presents an overview of the recent extensive fundamental studies on hydrogen embrittlement of high-Mn steels with aim towards obtaining a comprehensive understanding of the hydrogen embrittlement mechanisms in these materials. More specifically, we discuss four aspects: (1) microstructural cracking sites and crack growth pathways; (2) effects of segregation and its kinetics of interstitial atoms such as hydrogen and carbon; (3) alloying element effects and (4) microstructural and alloying approach for endowing these steels with better resistance against hydrogen embrittlement. All results presented in this overview were obtained at room temperature. All alloy compositions are given in weight percentage.

Microstructure effects assisting crack formation

Fig. 2a shows the characteristic hydrogen-induced degradation of the tensile ductility in an Fe-18Mn-0.6C austenitic

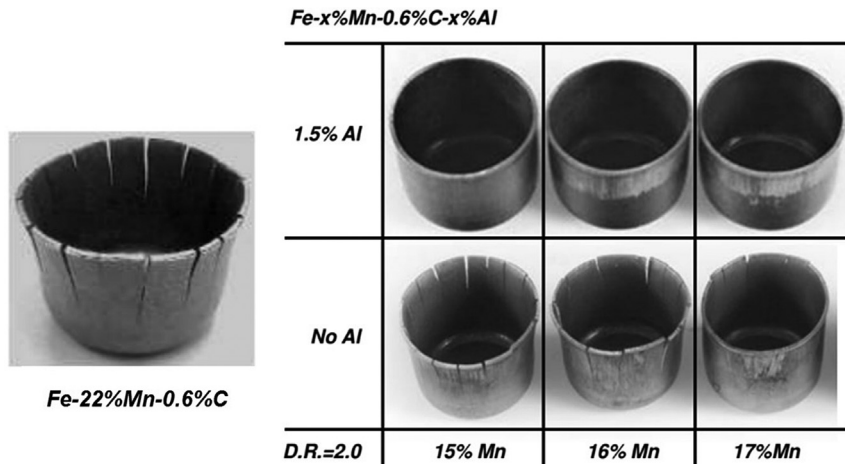


Fig. 1 – Hydrogen-induced delayed fracture in Al-free TWIP steel and its suppression by the addition of Al [26,46]. D.R.: drawing ratio. % refers to weight %. ©2011 De Cooman BC, Kim J, Chin K-G. Originally published by Intech in New trends and developments in automotive system engineering under CC BY-NC-SA3.0 license. Available from: DOI. 10.5772/552”.

TWIP steel when exposed to hydrogen. Hydrogen charging was carried out during tensile testing. Fracture occurred prior to the onset of plastic instability, indicating the occurrence of brittle fracture. The fracture mode of the hydrogen-charged specimens was primarily intergranular fracture (Fig. 2b). However, other fracture types can occur inside the martensite phase or along its interface with the austenitic matrix. Even when focusing on grain boundary cracking, the hydrogen-assisted intergranular cracking behavior depends on the microdamage density/distribution and micro-stress concentration spots that are gradually building up during the deformation-induced microstructural evolution, such as deformation twinning. In this section, we introduce details about the associated hydrogen-assisted cracking modes and the evolution of the specific deformation microstructure features that are relevant to hydrogen embrittlement.

Fig. 3a and b shows an example of hydrogen-assisted cracking associated with the presence of α' -martensite in an Fe-20Mn binary alloy. In austenitic steels with low stacking fault energy, α' -martensitic transformation occurs via ε -martensitic transformation [47,48]. This type of α' -martensitic transformation accommodates stress concentration at the ε -martensite plates and subsequently contributes to work hardening, which provides superior tensile ductility when hydrogen is not introduced [49,50]. However, in the presence of hydrogen, the increased metastability of the austenite against α' -martensitic transformation critically deteriorates the resistance to hydrogen embrittlement, as is well known for Fe-Cr-Ni austenitic stainless steels [41,42]. α' -martensite in high-Mn austenitic steels such as in the Fe-20Mn alloy also plays a negative role on the hydrogen embrittlement resistance, because of the occurrence of

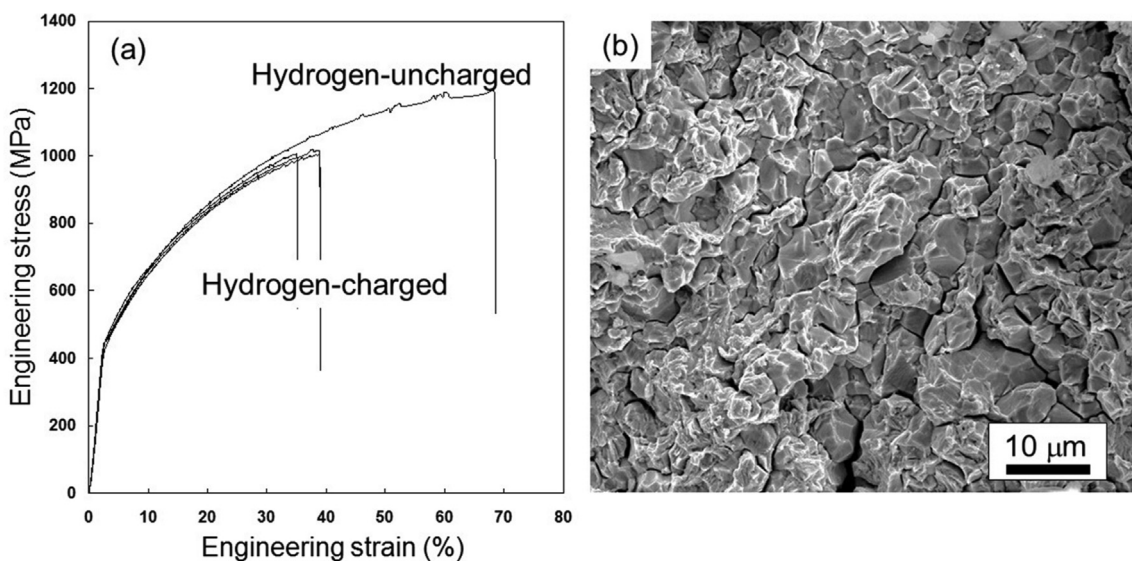


Fig. 2 – (a) Ductility degradation in a hydrogen-charged Fe-18Mn-0.6C TWIP steel. (b) Scanning electron micrograph showing an intergranularly fractured surface [24]. The initial strain rate is $5.1 \times 10^{-5} \text{ s}^{-1}$. Alloy composition is in weight %. “Reproduced with permission from Corros. Sci., 54, 1 (2012). Copyright 2011, Elsevier.”

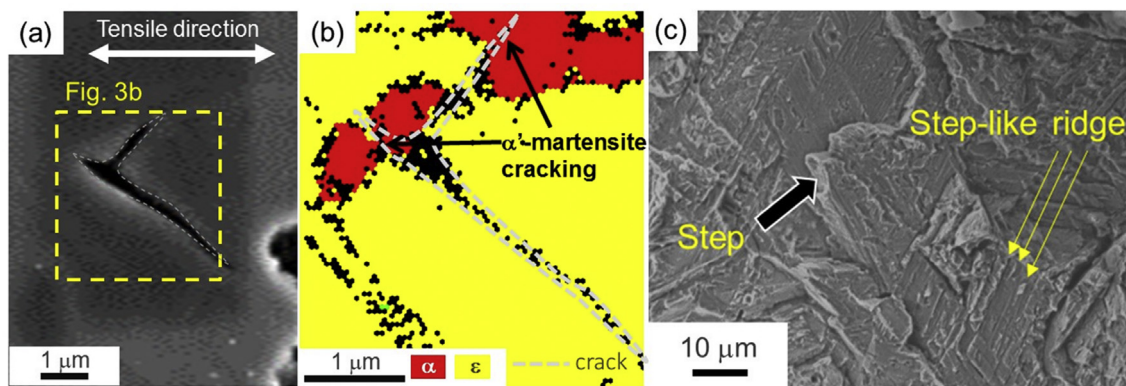


Fig. 3 – Hydrogen-assisted cracking in α' -martensite in an Fe-20Mn binary model alloy tested under hydrogen charging at a current density of 30 A/m^2 in a 3% NaCl + 3 g/L NH₄SCN aqueous solution [45]. (a) SEM image, (b) phase map obtained by electron backscatter diffraction pattern (EBSD) measurements, and (c) the associated fracture surface. The corresponding reduction in total elongation to fracture is shown later in the article in Fig. 19. Alloy composition is in weight %. “Reproduced with permission from Metall. Mater. Trans. A, 54, 2656 (2016). Copyright 2016, The Minerals, Metals & Materials Society and ASM International.”

cracking in or at the α' -martensite phase portions. Accordingly, the fracture surface forms in a quasi-cleavage fashion, as shown in Fig. 3c. Hydrogen-induced delayed fracture in some high-Mn steels such as Fe-16Mn-0.6C [46] and Fe-14Mn-0.7C-1.4Al [28] is also associated with α' -martensite formation.

Fig. 4a shows the hydrogen-related cracks in ϵ -martensite. Note that ϵ -martensitic transformation has been reported to cause premature fracture even without hydrogen charging [3,51–55]. Specifically, the pre-existing γ/ϵ interface, which is parallel to {111} _{γ} and {0002} _{ϵ} , interrupts secondary ϵ -martensite growth, which causes microstructural stress concentration at the secondary ϵ -martensite plate tip because of the low non-basal slip activity in ϵ -martensite. The microstructural stress concentration induces preferential crack initiation along the γ/ϵ interface [52]. Since the quasi-cleavage fracture occurs through the coalescence of microvoids/cracks

at the interface, the fracture surface contains step-like ridges. Hydrogen enhances the brittle-like behavior, inducing quasi-cleavage fracture, as shown in Fig. 4b. When the austenitic steel contains carbon, the hard ϵ -martensite is cracked more easily, resulting in a clearer quasi-cleavage feature [56], as shown in Fig. 4c. However, ϵ -martensite has a weaker effect on the hydrogen-related degradation of tensile ductility than the α' -martensite.

Fig. 5a shows hydrogen-assisted intergranular cracking in a κ -carbide or respectively cluster precipitation-hardened Fe-Mn-Al-C austenitic steel. These κ -carbides are few nm small and highly coherent non-oxidic perovskite precipitates which form in high Mn steels with elevated Al and C content after heat treatment [57,58]. The prevalent deformation mechanism of the precipitation-hardened austenitic steel is characterized by planar dislocation slip stemming from shearing

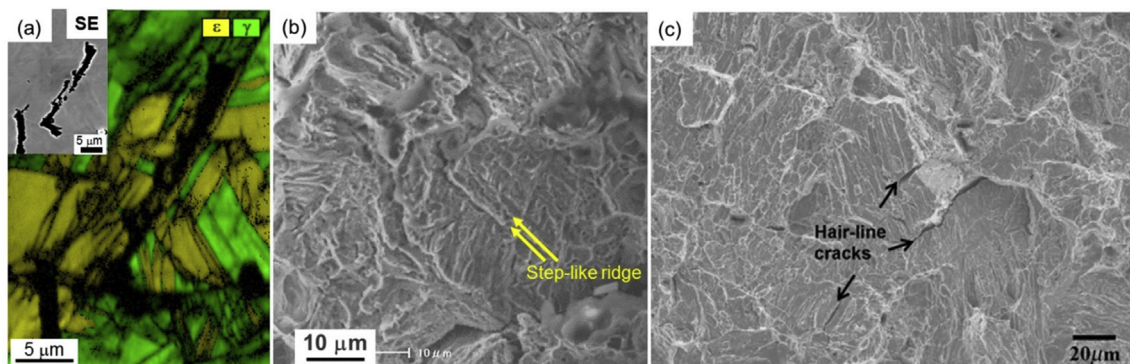


Fig. 4 – (a) EBSD phase map showing ϵ -martensite-related cracks and (b) its associated fracture surface in a hydrogen-charged Fe-28Mn alloy tested under hydrogen charging at a current density of 30 A/m^2 in a 3% NaCl + 3 g/L NH₄SCN aqueous solution [45]. Corresponding degradation in the total elongation to fracture is shown in Fig. 19. (c) Another example of quasi-cleavage fracture in a decarburized Fe-15Mn-2Cr-0.6C steel hydrogen-pre-charged at a current density of 60 A/m^2 in a 3% NaCl + 0.3% NH₄SCN aqueous solution [56]. Alloy compositions are in weight %. “Reproduced with permission from Metall. Mater. Trans. A, 54, 2656 (2016). Copyright 2016, The Minerals, Metals & Materials Society and ASM International and from Mater. Sci. Eng. A 533, 87 (2012). Copyright 2011, Elsevier.”

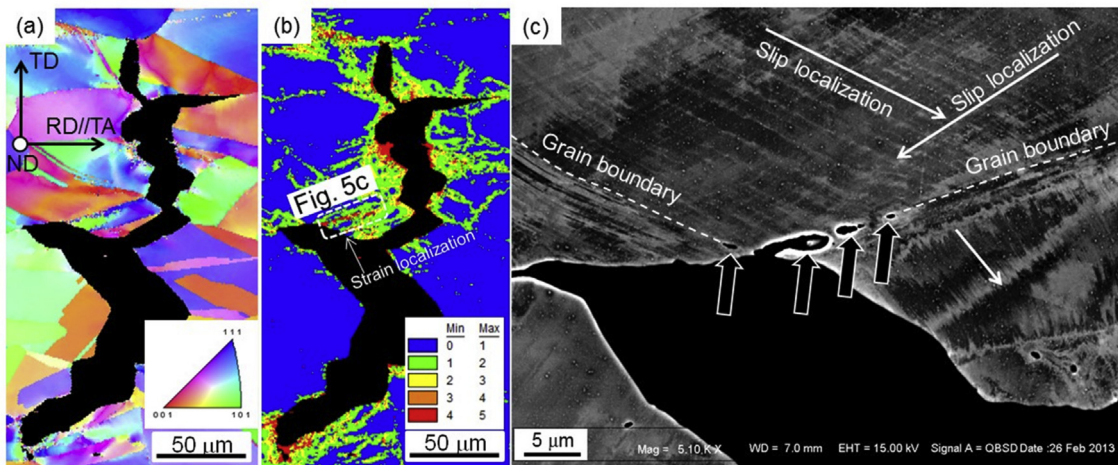


Fig. 5 – (a) Inverse pole figure (IPF) and **(b)** KAM maps with a hydrogen-induced intergranular crack in Fe-26Mn-11Al-1.2C austenitic steel containing κ -carbides tested under hydrogen charging at a current density of 10 A/m^2 , in a 3% NaCl + 3 g/L NH₄SCN aqueous solution. **(c)** Intergranular crack formation is induced by slip localization [72]. The elongation is reduced from 44% to 5% by hydrogen uptake. Alloy composition is given in weight % and deformation in the form of engineering strains. “Reproduced with permission from Int. J. Hydrogen Energy, 39, 4634 (2014). Copyright 2013, Elsevier.”

of the κ -carbides or respectively their precursor clusters [59–61]. This deformation characteristic plays an important role in the intergranular cracking due to strain localization at grain boundaries. Fig. 5b shows the Kernel average misorientation (KAM) map, which serves as a qualitative measure for the lattice curvature related plastic strain distribution [62]. The region outlined by the broken line indicates regions of plastic strain localization around a grain boundary. This part is magnified by the electron channeling contrast imaging (ECCI) technique in Fig. 5c. In the ECCI images, grains with an optimized Bragg contrast appear dark because of the low intensity of the backscatter electron emission [63,64]. Lattice defects, microstructure interfaces, twins, and the second phase locally affect the channeling contrast, and hence are visualized in bright contrast. The white lines in Fig. 5c indicate localized slip bands. The slip localization apparently induces micro-void formation along the grain boundaries, which in turn promotes grain boundary cracking. Slip localization in this type of steel is enhanced by hydrogen uptake [65] and the associated hydrogen-enhanced localized plasticity (HELP) [66–68], assisting ductile fracture along the grain boundaries. More specifically, such confined and hydrogen-enhanced plasticity [66–68] is suggested to result in an increased density of deformation-related vacancies, which are further stabilized by instantaneous decoration by the abundant hydrogen [69,70]. These vacancies can then condensate at the grain boundaries and at microband or respectively slip band intersections to form hydrogen decorated, and hence stable, nanovoids, which undergo gradual coalescence [71].

In addition to the effects associated with martensite and slip localization, twin boundaries also play a crucial role in hydrogen-assisted cracking. Particularly in TWIP steels, deformation twins are intrinsically unavoidable, and hence, understanding their influence on the underlying hydrogen embrittlement mechanisms is essential. A corresponding discussion is presented in the ensuing section.

Importance of $\Sigma 3$ twin boundary: coherency and segregation

Twin boundary cracking occurs in austenitic steels, particularly in those with a high Mn content [73–77], as shown in Fig. 6a. The crack propagates in a zigzag shaped manner along the primary and secondary deformation twins. Twin boundary cracking at cryogenic temperatures has been reported before in austenitic stainless steels even without the presence of hydrogen [78,79]. Such phenomena were attributed to micro-stress concentrations occurring at the twin plate tips adjacent to obstacle twin boundaries [78,79]. Moreover, deformation twinning is generally known to assist intergranular cracking [75,80,81]. Specifically, impingement of deformation twin plates at grain boundaries may result in intergranular crack initiation and propagation (Fig. 6b). Accordingly, the fracture surface of hydrogen-charged TWIP steels shows intergranular or quasi-cleavage features, as depicted in Figs. 2b and 6c. The quasi-cleavage fracture surface contains fine plate-like surface relieves (Fig. 6c) which is due to the interaction between localized slip features and twin boundaries. In addition, secondary cracks are often observed on the fracture surface of hydrogen-charged TWIP steels due to crack branching along other deformation twin boundaries [73]. Since deformation twinning is required to gain superior mechanical properties when hydrogen is not introduced, the negative effect of twinning is unavoidable and acts as a major factor that causes the hydrogen-assisted cracking in high-Mn TWIP steels.

For explaining why twin boundary cracking occurs preferentially in hydrogen-charged TWIP steel, the probability of hydrogen segregation at the $\Sigma 3$ twin boundaries must be taken into consideration. According to *ab initio* simulations (Fig. 7), hydrogen atoms have a repulsive interaction with $\Sigma 3$ coherent twin boundaries. In contrast, thermal desorption

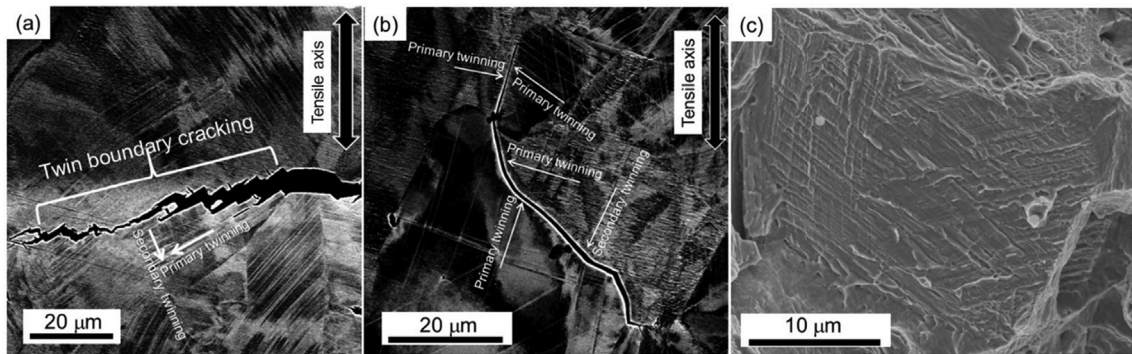
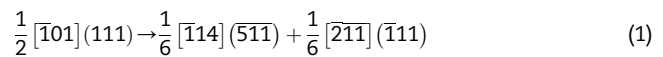


Fig. 6 – Hydrogen-assisted cracking (a) along deformation twin boundaries and (b) twinning-enhanced hydrogen-assisted intergranular cracking in an Fe-18Mn-1.2C TWIP steel tested under hydrogen charging at a current density of 9 A/m², in a 3% NaCl + 3 g/L NH₄SCN aqueous solution [75]. (c) A fracture surface pertaining to twin boundary cracking in Fe-23Mn-0.5C TWIP steel hydrogen-pre-charged with high pressure (7.3 MPa) hydrogen gas [90]. Alloy compositions are given in weight %. “Reproduced with permission from Acta Mater., 61, 4607 (2013). Copyright 2013 Elsevier, and from Int. J. Hydrogen Energy 41 15362 (2016). Copyright 2016, Elsevier.”

analysis (TDA) [20], hydrogen micro-printing (Fig. 8a) [76], and scanning Kelvin probe force microscopy (SKPFM) (Fig. 8b–d) [82] analyses have clarified that hydrogen segregates on twin boundaries or within deformation twin plates. For instance, the potential map and profile obtained by the SKPFM indicate that hydrogen preferentially exists at deformation twins, as indicated by the black arrows and dotted square in Fig. 8b. The hydrogen segregation which was in the beginning created by hydrogen charging disappeared gradually with aging time at room temperature as hydrogen desorption was gradually accomplished (Fig. 8c and d). This discrepancy between the theoretical and experimental analyses can be associated with the high lattice defect density at or along the deformation twins [76] and the incoherency on the $\Sigma 3$ twin boundaries [75]. Hydrogen has been reported to segregate particularly to defected twin boundaries [83,84]. Specifically, tritium, a heavy radioactive isotope of hydrogen, appears to segregate at the corners of the steps on the twin boundaries in austenitic steel [84]. Atomistic defects such as steps along the twin boundary

plane are easily formed by plastic deformation. Plastic deformation causes interactions between the dislocation and the twin boundary through dislocation dissociation [80,85–87]. An example of such a reaction is for instance [85],



where the $(\overline{1}11)$ plane is the obstacle twin boundary. The formation of $1/6[\overline{2}11]$ dislocations creates slip steps on the obstacle twin boundary [88], disturbing its coherency. A possible mechanism underlying hydrogen-assisted cracking at twin boundaries is schematically illustrated in Fig. 9. Accordingly, a primary twin boundary is first formed (step 1), which is then distorted by hydrogen-enhanced slip [68,89] and secondary twinning (step 2). The distorted twin boundaries, such as the corners or respectively ledges of the steps, can then trap hydrogen (step 3). The subsequently formed secondary twins and the slip dislocation pile-up cause microstructural stress concentrations on the twin boundaries (step

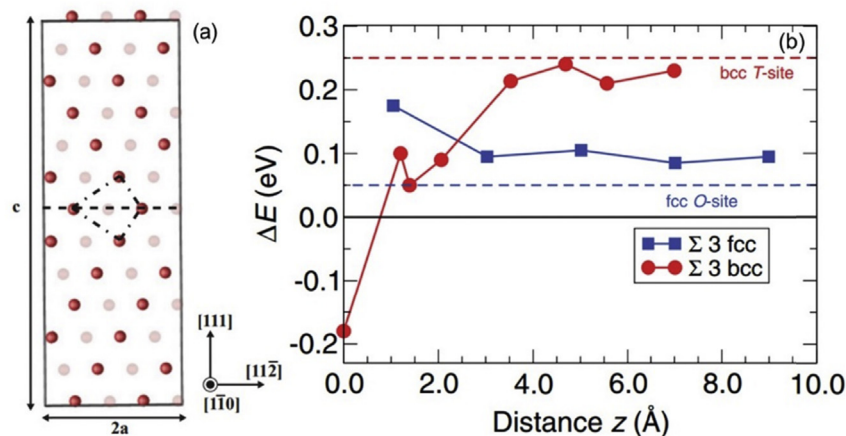


Fig. 7 – Ab initio simulation of hydrogen–grain boundary interaction in bcc and fcc iron crystal structure [91]. (a) Atomistic model of $\Sigma 3$ boundary in fcc iron. (b) Solution energies of hydrogen plotted against distance from $\Sigma 3$ grain boundaries. bcc: body centered cubic; fcc: face centered cubic. “Reproduced with permission from Phys. Rev. B, 84, 144121 (2011). Copyright 2011, American Physical Society.”

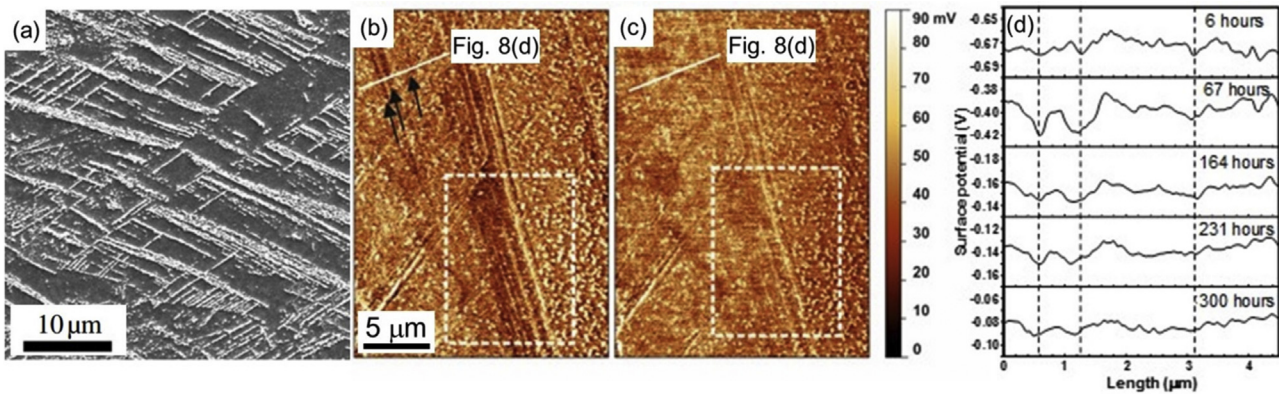


Fig. 8 – Hydrogen segregation at deformation twin plates revealed by (a) hydrogen microprint (Fe-18Mn-0.6C TWIP steel deformed by 30% strain) [76] and scanning Kelvin probe force microscopy at exposure times at room temperature for (b) 67 and (c) 300 h (Fe-18Mn-1.2C TWIP steel deformed by 30% strain). The SKPFM results are presented as surface potential maps; the potential decreases with increasing hydrogen content [92]. Locally low potential is observed in the region indicated by black arrows and dotted square. This feature subsequently disappeared during aging when the hydrogen left the specimen. (d) Exposure time-dependent variation of line profiles corresponding to the white lines in Fig. 8(b) and (c) [82]. Alloy compositions are given in weight % and deformation in the form of engineering strains. “Reproduced with permission from Proc. Roy. Soc. A, 469, 20120458 (2012). Copyright 2012 The Royal Society, and from J. Electrochem. Soc., 160, C643 (2015). Copyright 2015, The Electrochemical Society.”

4). When the stress concentration cannot be accommodated plastically because of a reduction in the cohesive energy resulting from the presence of hydrogen, twin boundary cracking occurs (step 5).

Strain rate dependence: Kinetic Effects associated with hydrogen and carbon

Fig. 10 shows that the hydrogen embrittlement susceptibility increases with decreasing strain rate in an Fe-23Mn-0.5C TWIP steel. Based on the process of hydrogen-assisted cracking suggested in Fig. 9, hydrogen segregation and hydrogen-decorated dislocation motion are key effects describing the strain rate dependence of the material's tensile ductility when exposed to hydrogen. In step 2 of Fig. 9, hydrogen-enhanced localized slip resulting in steps on the twin boundaries is enhanced when decreasing the strain rate, because of the competitive motion of dislocations and diffusible hydrogen [93–95]. In step 3, a decrease in the strain rate results in an increase in waiting time for hydrogen segregation. Moreover, at a low strain rate, hydrogen-decorated dislocation motion would deliver hydrogen atoms to the twin boundary. Since the cohesive energy depends on the segregated hydrogen content on the twin boundary, the hydrogen delivery by the strain-

rate-dependent motion resulting from the hydrogen-decorated dislocation is crucial. Consequently, the hydrogen embrittlement susceptibility of the TWIP steel markedly increased with decreasing strain rate.

In addition to the kinetic role of hydrogen and its relation to the dislocation velocity, the motion of interstitial carbon is also important in the context of strain rate effects in Fe-Mn-C austenitic steels [44,96]. This is due to the fact that carbon in high-Mn austenitic steels causes static and dynamic strain aging, which affects strain localization [97,98], work hardening [99,100], and static strength [101,102]. Fig. 11 shows the “pre-strain rate” dependence of hydrogen-induced delayed fracture behavior in an Fe-22Mn-0.6C TWIP steel. In this experiment, as shown in Fig. 11a, tensile deformation conducted at different pre-straining rates without any hydrogen charging was stopped at 69% engineering strain. After this initial pre-straining the specimen was charged with hydrogen at a fixed cross-head displacement. If hydrogen-induced fracture did not occur within 10 h, the specimen was deformed again until fracture. Since dynamic strain aging is enhanced by decreasing strain rate in these steels, the effect of strain aging by carbon on the flow stress increases with decreasing pre-straining rate. Accordingly, the stress level at the fixed cross-head displacement increases with decreasing pre-straining rate. Fig. 11b shows that hydrogen-induced

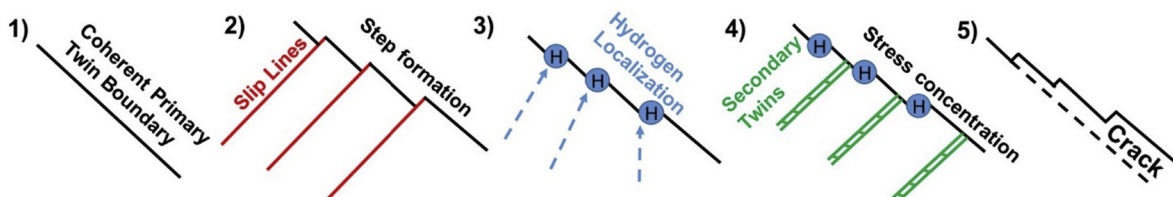


Fig. 9 – Schematic of a sequential process of defect formation, hydrogen segregation, twinning-induced stress concentration, and cracking [90].

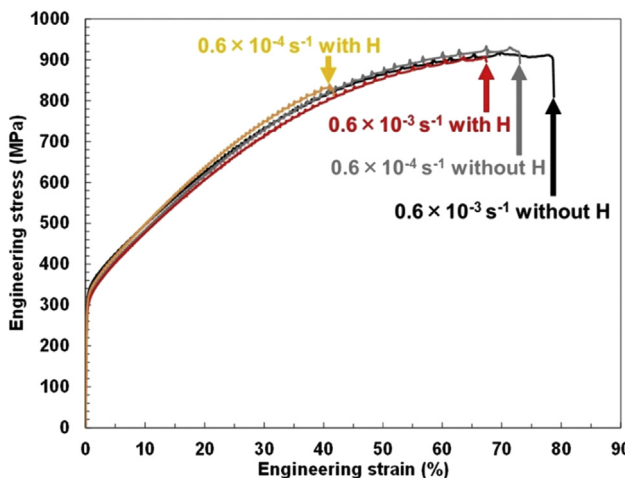


Fig. 10 – Strength and elongation decrease with decreasing strain rate in an Fe-23Mn-0.5C TWIP steel pre-charged with 7.3 MPa high-pressure hydrogen gas [90]. Alloy composition is given in weight %.

delayed fracture takes place at low pre-straining rates, i.e., 1.7×10^{-5} and $1.7 \times 10^{-4} \text{ s}^{-1}$. In contrast, the hydrogen-induced delayed fracture did not occur at strain rates of 1.7×10^{-3} and $1.7 \times 10^{-2} \text{ s}^{-1}$. In fact, regarding time to fracture, the hydrogen-induced delayed fracture was suppressed by increasing pre-straining rate. The change in the hydrogen embrittlement susceptibility can be explained by the increase in the stress level with decreasing pre-straining rate because of the enhanced dynamic strain aging as mentioned above. In addition, depinning of dislocations that were pinned in a solute carbon atmosphere would cause localized slip because of local softening on a specific slip plane [97]. This effect would enhance hydrogen effects such as crack propagation accelerated by the HELP mechanism at a crack tip in a strain-aged TWIP steel [96].

Effects of Al on hydrogen uptake and embrittlement behavior

According to TDA results, a considerable amount of hydrogen can be introduced into binary Fe-Mn austenitic alloys and also into ternary Fe-Mn-C TWIP steels. In either case the fracture strength decreases with increasing diffusible hydrogen content [32,103]. Similar as in conventional high-strength steels such as martensitic steels, the diffusible hydrogen atoms in high-Mn austenitic steels are getting trapped at various types of microstructural sites, e.g., dislocations [20], incoherent grain boundaries [20], twin boundaries [20], VC [104], TiN [105], or at κ carbides [72]. All these defect decoration phenomena can affect the relationship between the material's hydrogen content and its fracture strength. As pointed out in a previous review paper [106], the control and suppression of both, hydrogen uptake and its distribution via adequate microstructure design measures provide key approaches for reducing the hydrogen embrittlement susceptibility of steels.

Instead of the introduction of such microstructural hydrogen trap sites, diffusible hydrogen uptake of high-Mn TWIP steels can be prevented by the addition of Al [32,33] (Fig. 12a), which clearly suppresses hydrogen embrittlement and the associated delayed fracture phenomenon as shown in Fig. 1. Therefore, the effect of Al on hydrogen uptake has drawn attention as one of the most essential research topics related to TWIP steels. However, the Al addition not only suppresses hydrogen uptake, but also decreases its embrittlement sensitivity to diffusible hydrogen content as shown in Fig. 12b [32]. A quantitative relationship between the diffusible hydrogen content and fracture stress in a specific experimental condition in Fe-18Mn-xAl TWIP steels has been described as follows.

$$\sigma_f = 2000[H]_D^{-0.132 \exp\left(-\frac{[Al]}{1.125}\right)} \quad (2)$$

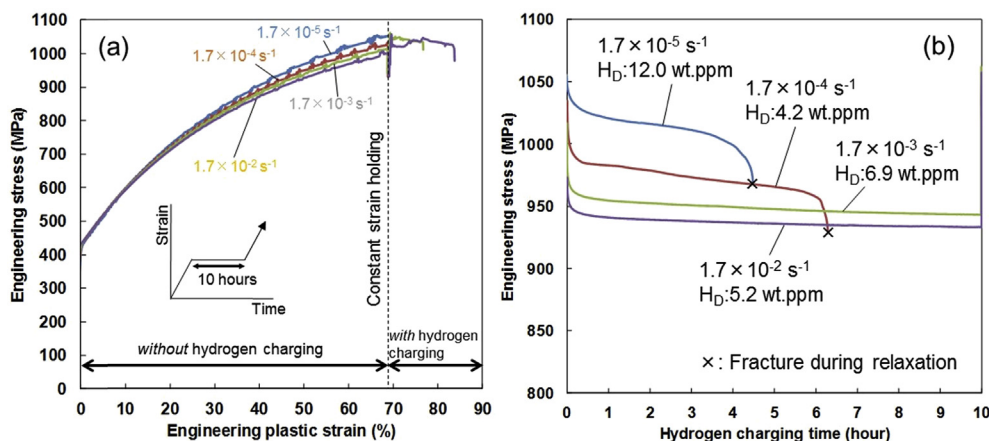


Fig. 11 – Pre-straining rate dependence of time to hydrogen-induced delayed fracture in an Fe-22Mn-0.6C TWIP steel [44]. (a) Engineering stress–strain curves with different strain rates and subsequent cross-head displacement holding. (b) Engineering stress plotted against holding time that equals the hydrogen charging time. H_D : diffusible hydrogen content. The hydrogen charging was carried out at a current density of 7 A/m^2 in a 3% NaCl aqueous solution containing 3 g/L of NH_4SCN at a fixed cross head position. Alloy composition is given in weight %. “Reproduced with permission from Scripta Mater., 66, 947 (2012). Copyright 2012 Elsevier.”

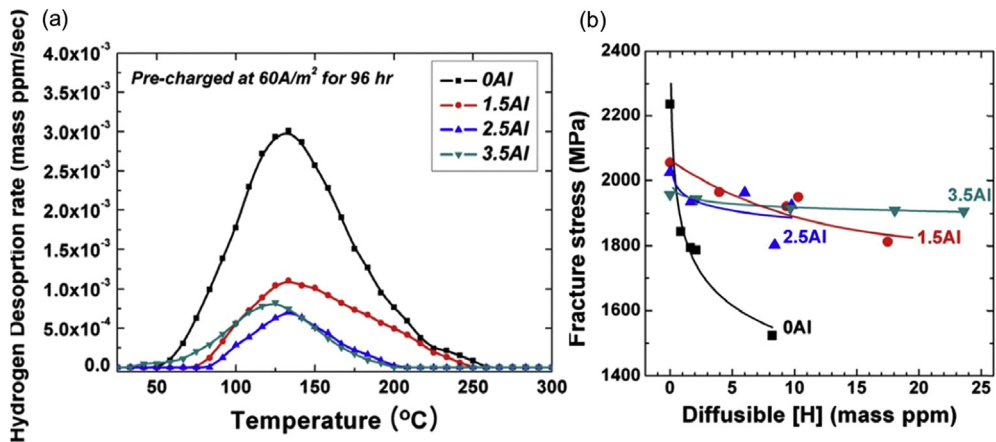


Fig. 12 – (a) TDA profiles with different Al contents in Fe-18Mn-xAl TWIP steels at an identical hydrogen charging condition. **(b)** Fracture stress of notched specimens plotted against diffusible hydrogen content obtained from Fig. 12a [32]. Alloy compositions are given in weight %. “Reproduced with permission from Scripta Mater., 66, 960 (2012). Copyright 2012 Elsevier.”

where $[H]_D$ and $[Al]$ are in wt.ppm and wt.%, respectively. For revealing the effect of Al on the hydrogen embrittlement susceptibility of high-Mn steels, we must consider the mechanism of hydrogen uptake suppression and the predominant factors determining the relationship expressed by Eq. (2).

First, we explain the suppression mechanism of hydrogen uptake through the addition of Al. One aspect to consider is that the solubility of hydrogen has been reported to increase with the solute Al content [107,108]. Furthermore, the

suppression of hydrogen uptake has been associated with the prevention of hydrogen entry from a specimen surface into the bulk [109] and the deterioration of hydrogen diffusivity in a bulk specimen [107,108]. A promising reason why hydrogen uptake could be hampered or even prevented by an increase in the Al content is the formation of an Al_2O_3 surface layer. As shown in Fig. 13a, the Al_2O_3 layer homogeneously forms between the specimen surface and the general oxidation layer when Al is added to TWIP steels. The Al_2O_3 layer can be formed through chemical reactions between metallic atoms

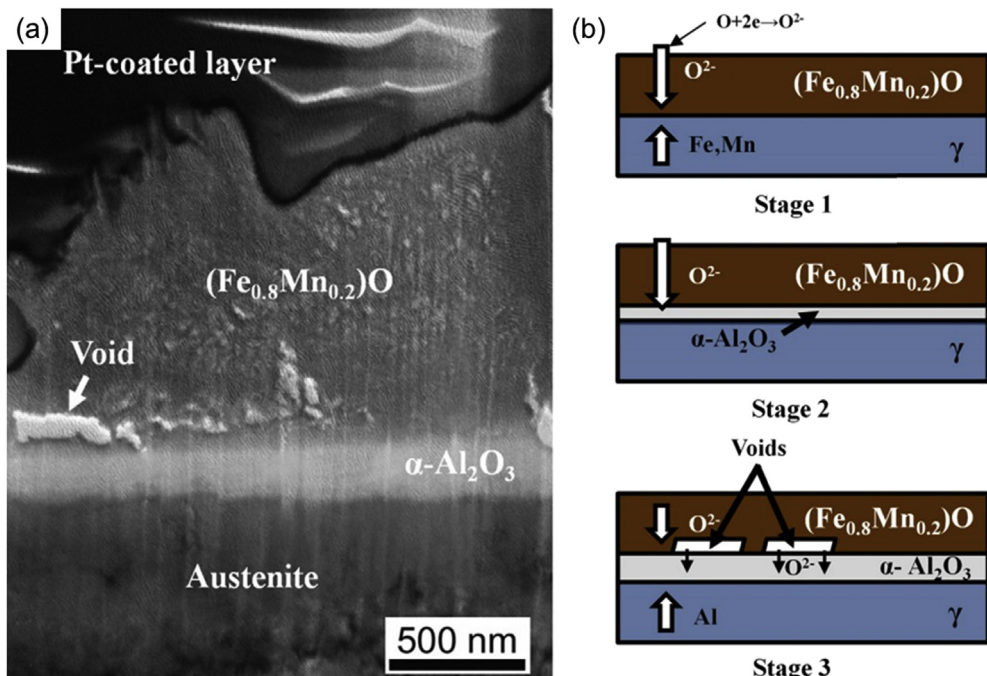


Fig. 13 – (a) Transmission electron micrograph showing Al_2O_3 layer formation on a specimen surface of an Fe-18Mn-0.6C-1.5Al TWIP steel. **(b)** Schematics for the formation process of the Al_2O_3 layer [109]. Alloy composition is given in weight %. “Reproduced with permission from Int. J. Hydrogen Energy, 37, 9925 (2012). Copyright 2012 Elsevier.”

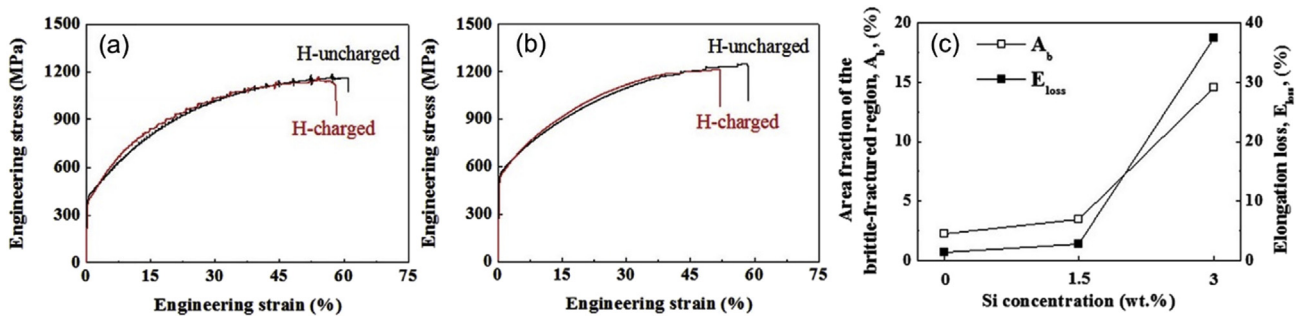


Fig. 14 – Effect of Si on hydrogen embrittlement susceptibility in (a) Fe-18Mn-0.6C and (b) Fe-18Mn-0.6C-1.6Si steels pre-hydrogen-charged at a current density of 50 A/m^2 in a $3\% \text{ NaCl} + 0.3\% \text{ NH}_4\text{SCN}$ aqueous solution. (c) Si concentration dependence of area fraction of the brittle-fracture region and elongation loss [115]. The initial strain rate is $4.8 \times 10^{-5} \text{ s}^{-1}$. Alloy compositions are given in weight %. “Reproduced with permission from *Acta Mater.*, 103, 264 (2016). Copyright 2015 Elsevier.”

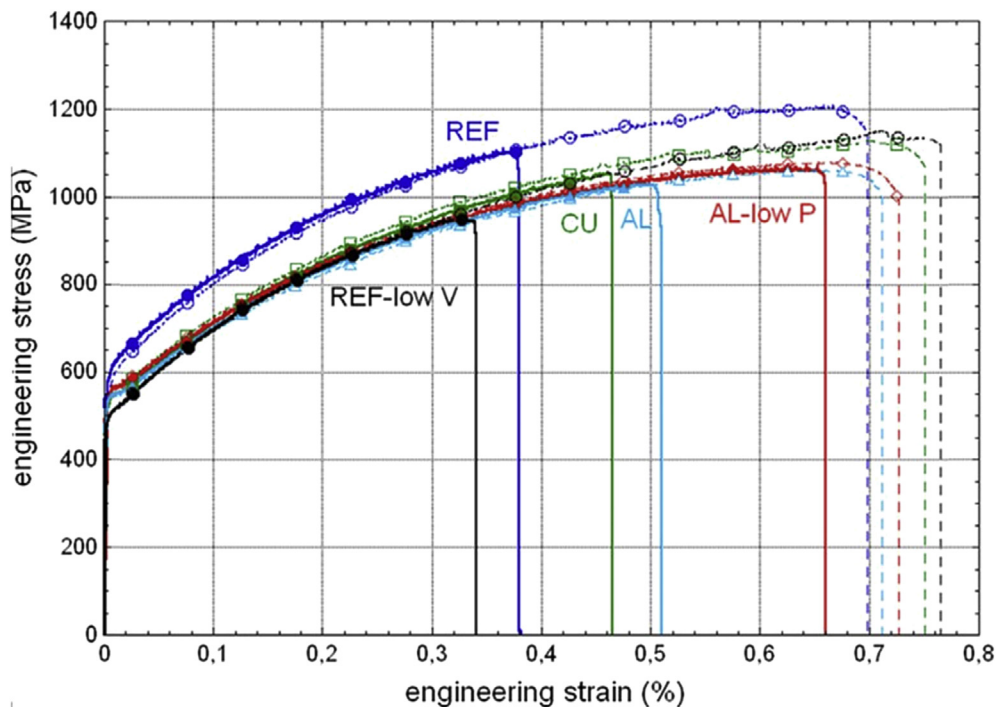


Fig. 15 – Effects of Cu and P on hydrogen embrittlement susceptibility in Fe-18Mn-0.6C-based TWIP steels tested under hydrogen charging at a current density of 10 A/m^2 in a 0.1 M NaOH aqueous solution [43]. Stress–strain curves without hydrogen charging are shown as dotted lines. The initial strain rate is 10^{-4} s^{-1} . The detailed chemical compositions are listed in Table 1. REF: reference grade steel. Alloy composition is given in weight %. “Reproduced with permission from *Corros. Sci.*, 82, 218 (2014). Copyright 2014 Elsevier.”

and the environmental oxygen [109]. Fe and Mn ions are firstly oxidized to $(\text{Fe}0.8\text{Mn}0.2)\text{O}$ on the specimen surface (Stage 1 in Fig. 13b). Since the porous $(\text{Fe}0.8\text{Mn}0.2)\text{O}$ layer cannot act as a sufficiently strong barrier to the permeation of O^{2-} ions, O^{2-} ions diffuse further through the oxide layer and accumulate underneath the $(\text{Fe}0.8\text{Mn}0.2)\text{O}$ layer, where the Mn was depleted. Then, the O^{2-} ions combine with Al, which forms the Al_2O_3 layer (Stage 2 in Fig. 13b). The voids revealed in Fig. 13a are initiated at the interface between $(\text{Fe}0.8\text{Mn}0.2)\text{O}$ and an Al_2O_3 layer by the one-way diffusion of O^{2-} ions from

Table 1 – Chemical compositions of the steel used in Fig. 14 [43] in weight %.

Grade	Fe	C	Mn	V	Cu	P	Al
REF	Base	0.6	18.1	0.2		0.032	
REF-low V	Base	0.6	18.4			0.032	
CU	Base	0.6	17.9	0.2	1.7	0.031	
AL	Base	0.6	16.9	0.2		0.037	1.5
AL-low P	Base	0.6	17.1	0.2		0.005	1.5

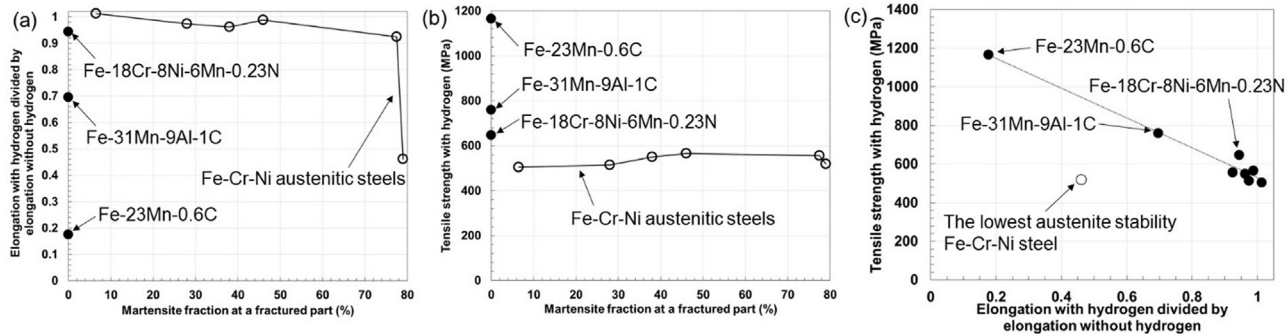


Fig. 16 – Hydrogen embrittlement susceptibility of high-Mn steels in a 10 MPa high-pressure hydrogen gas atmosphere [30,118]. (a) Magnitudes of hydrogen-degraded elongation and (b) tensile strength with hydrogen plotted against martensite fraction at a fractured part. (c) The tensile strength in Fig. 16(b) is plotted against the degradation magnitudes of elongation shown in Fig. 16(a).

the (Fe0.8Mn0.2)O layer to the Al₂O₃ layer. This void formation provides effective pathways for the permeation of O²⁻ ions to form the Al₂O₃ layer (Stage 3 in Fig. 13b). In addition, considering the other factor mentioned above, Al addition has been theoretically and experimentally shown to deteriorate hydrogen diffusivity [107,108]. Therefore, the average hydrogen content of an Al-added high Mn steel can be decreased at a limited hydrogen charging time because of the hydrogen-affected layer being thinner than that in the case of a steel composition without Al addition. The combined effect of the Al₂O₃ layer and the diffusivity deterioration is the reason why hydrogen uptake is prevented by Al addition.

In terms of the embrittlement sensitivity to diffusible hydrogen shown in Eq. (2), Al plays also multiple roles in the suppression of hydrogen embrittlement. As mentioned above, martensitic transformation, deformation twinning, and strain aging all assist in the occurrence of hydrogen-assisted cracking. Al, when alloyed in sufficient quantity, suppresses the α' -martensitic transformation [46,110]. An increase in the stacking fault energy caused by the Al addition suppresses ϵ -martensitic transformation [46] and deformation twinning [111,112] as well. In addition, the increase in the stacking fault energy and an increase in the activation energy for carbon diffusion strongly prevent the occurrence of strain aging [96,100,113]. An additional effect of the increase in the stacking fault energy is that cross slip occurs more easily, which inhibits dislocation pile-ups and associated localized dislocation transport of hydrogen. Furthermore, Al addition tends to reduce the effect of hydrogen-enhanced elastic/plastic deformability [114]. Hence, the Al addition counteracts most of the above discussed negative microstructural factors simultaneously, which drastically decreases the hydrogen embrittlement susceptibility of high-Mn steels.

Effects of alloying elements Mn, Si, Cu, and P in high-Mn steels

Most recent works on hydrogen embrittlement in high-Mn austenitic steels have been carried out for typical TWIP steel compositions such as Fe-Mn-C or Fe-Mn-Al-C systems. However, it is also interesting how other alloying elements affect

hydrogen embrittlement susceptibility in high-Mn austenitic steels. In fact, in addition to the Al effect, the influencing effects of Mn [45], Si [115], Cu [43], and P [43] in solid solution states have been investigated systematically also.

The Mn effect was examined by using binary Fe-Mn austenitic alloys [45]. As is well known, Mn increases the stability of the austenite phase, which decreases hydrogen embrittlement susceptibility since both, the trend towards twin and towards martensite formation are reduced. However, when austenite is fully stable, excess Mn assists in the intergranular cracking probably because of a reduction in the cohesive energy of grain boundaries [116,117].

Fig. 14 shows the effect of Si on the hydrogen embrittlement susceptibility in an Fe-18Mn-0.6C TWIP steel. The addition of 1.6%Si increases the hydrogen embrittlement susceptibility as revealed when comparing Fig. 14a and b [115]. Further addition of Si results in a considerable amount of deformation-induced

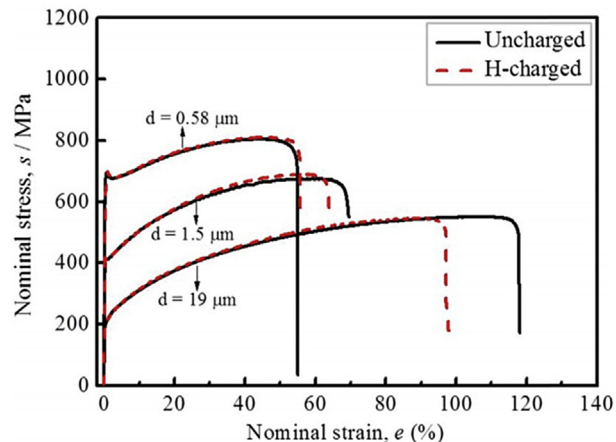


Fig. 17 – Impact of grain refinement on hydrogen embrittlement in an Fe-31Mn-3Al-3Si TWIP steel
hydrogen-pre-charged at 100 A/m² in a 3% NaCl aqueous solution containing 3 g/L of NH₄SCN [121]. The initial strain rate is 8.3×10^{-6} s⁻¹. Alloy composition is given in weight %. “Reproduced with permission from Mater. Sci. Eng. A, 651, 935 (2016). Copyright 2015 Elsevier.”

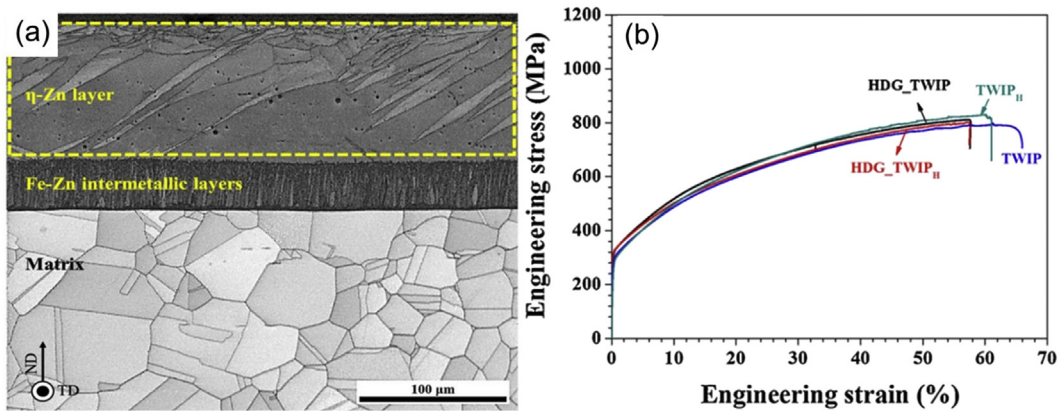


Fig. 18 – (a) SEM micrographs of the Fe-18Mn-0.6C-2Al TWIP steel hot-galvanized with Zn. **(b)** Tensile behavior of the hot-galvanized steel with and without hydrogen charging [122]. Alloy composition is given in weight %. “Reproduced with permission from Corros Sci., 111, 267 (2016). Copyright 2016 Elsevier.”

ϵ -martensite, which causes distinct hydrogen-induced deterioration of the elongation to fracture pertaining to the occurrence of brittle fracture as shown in Fig. 14c.

Fig. 15 demonstrates the effects of Cu and P on the hydrogen embrittlement susceptibility in an Fe-18Mn-0.6C TWIP steel. Cu addition suppresses the hydrogen effect on the elongation to fracture. Similar to the Al effect, Cu also increases the stacking fault energy, which contributes to the decrease in hydrogen embrittlement susceptibility [43]. On the other hand, the P effect in the Al-added TWIP steels critically increases the hydrogen embrittlement susceptibility. In fact, the elongation to fracture of a TWIP steel without Al does not drop by the presence of P [43]. Thus, the presence of P counteracts the positive effect of Al on the hydrogen embrittlement resistance, resulting in higher embrittlement susceptibility of the Fe-Mn-Al-C TWIP steel. The underlying mechanism of the impurity effect of P on hydrogen embrittlement still needs to be further investigated in future.

Embrittlement behavior in hydrogen gas atmospheres

Understanding embrittlement susceptibility in high-pressure hydrogen gas atmospheres is crucial for application to hydrogen-energy-related infrastructures. As shown in Fig. 16, a systematic study in a 10 MPa high-pressure hydrogen gas atmosphere has been conducted for metastable and stable austenitic steels. As seen in Fig. 16a, high-Mn stable austenitic steels show high hydrogen embrittlement susceptibility, even compared to metastable Fe-Cr-Ni stainless steels. This is due to the combined effect of multiple factors mentioned above (formation of deformation twins, grain boundary cohesive energy with high Mn content, strain age hardening). However, note that the high-Mn steels presented here exhibit markedly high tensile strength even in a hydrogen atmosphere, as shown in Fig. 16b. Fig. 16c shows the relationship between the

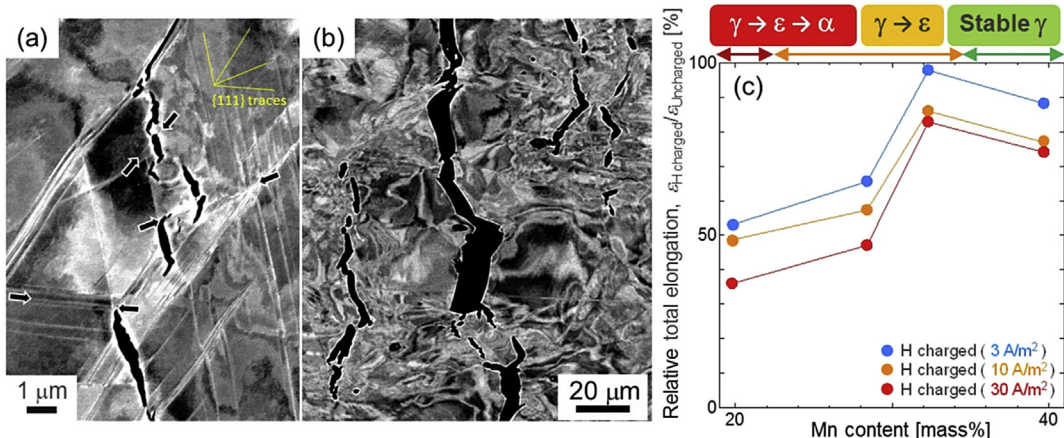


Fig. 19 – Damage arrest associated with hydrogen-assisted cracking in an Fe-32Mn binary alloy [45]. **(a)** Micro-damage arrest at thin ϵ -martensite plates. **(b)** A considerable number of cracks are arrested through crack blunting. **(c)** Mn-content dependence of hydrogen-induced ductility reduction in Fe-Mn binary alloys. Alloy compositions are given in weight %. “Reproduced with permission from Metall. Mater. Trans. A, 54, 2656 (2016). Copyright 2016, The Minerals, Metals & Materials Society and ASM International.”

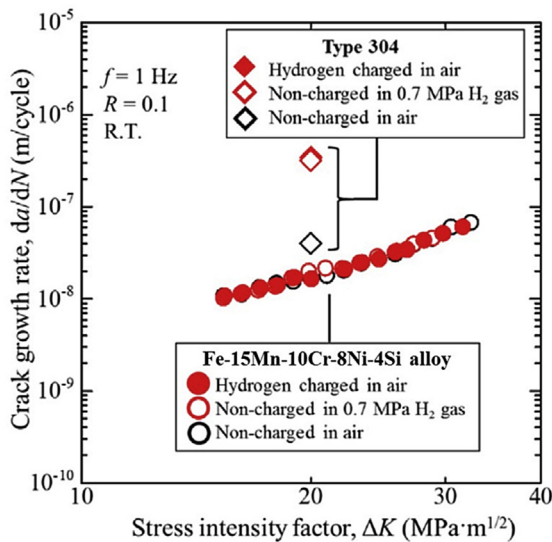


Fig. 20 – Fatigue crack growth under hydrogen gas environment in an Fe-15Mn-10Cr-8Ni-4Si alloy that shows deformation-induced ϵ -martensitic transformation [123]. The results for a type 304 austenitic steel (Fe-18Cr-8Ni stainless steel) which shows deformation-induced α' -martensitic transformation, are presented as reference data. Alloy compositions are given in weight %. “Reproduced with permission from *Scripta Mater.*, 113, 6 (2016). Copyright 2015, Elsevier.”

degradation magnitudes of elongation and the tensile strength under the effect of hydrogen. The relationship can be approximated by a linear function, except in the case of the Fe-Cr-Ni steel with the lowest austenite stability. This implies that the increased strength is the primary factor responsible for the distinct degradation of elongation in high-Mn steels under a high-pressure hydrogen gas atmosphere. In other words, high-Mn steels are potential next-generation materials for application to hydrogen-energy-related infrastructures when a strength level exceeding that of Fe-Cr-Ni austenitic steels is required. For realizing this application, the microstructure and chemical composition must be further optimized on the basis of the factors introduced in this paper.

Ways to enhance hydrogen degradation resistance

As mentioned above, Al addition is the most effective solution to improve the hydrogen embrittlement resistance of high-Mn austenitic steels. As alternative solutions, the hydrogen embrittlement susceptibility of high-Mn austenitic steels can be reduced by grain refinement [119–121], optimal Zn surface coating [122], enhancement of the damage arrest property [45], and optimal utilization of ductile ϵ -martensite formation for the case of fatigue loading [123].

Fig. 17 shows an example of the grain size dependence of the tensile behavior of specimens with and without hydrogen charging. The tensile strength increases with decreasing grain size and the grain refinement also suppresses hydrogen-induced degradation of the tensile mechanical properties. The positive effect of grain refinement can be explained in terms of three factors. First, the grain refinement suppresses deformation twinning [119,120,124]. Second, it reduces the diffusible hydrogen content per grain boundary area [119]. Third, the frequency of local stress concentration spots at grain boundaries decreases with decreasing grain size, which may also affect the local hydrogen content at grain boundaries [121].

The next improvement strategy lies in adding a Zn surface coating onto the steel. Zn surface coatings cause liquid metal embrittlement, which deteriorates ductility [125,126]. However, when the coating condition is optimal, it suppresses hydrogen embrittlement. An example of a hot-galvanized TWIP steel is shown in Fig. 18a. The Zn coating layer consists of η -Zn and Fe-Mn intermetallic layers. Although hot galvanization reduces ductility by 10% strain in Fig. 18b, hydrogen is trapped at the η -Zn and the Fe-Zn intermetallic layers, preventing the occurrence of hydrogen embrittlement.

The third strategy is based on damage arrest. In general, even if hydrogen-assisted damage initiates, it can be arrested through damage tip blunting at specific microstructures in multi-phase steels [127,128]. Although numerous or brittle ϵ -martensite plates deteriorate resistance against hydrogen embrittlement as mentioned above, a small amount of ductile ϵ -martensite in high-Mn steels act as a microstructure feature which is capable of arresting damage incidents as shown in

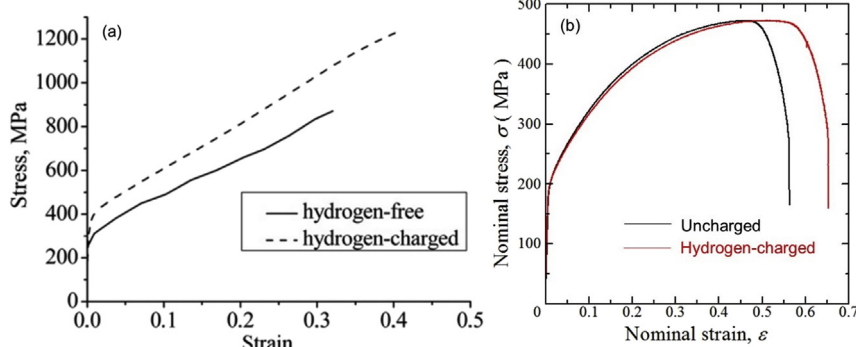


Fig. 21 – Positive utilization of solute hydrogen (a) in a single-crystalline Fe-13Mn-1.0C Hadfield steel with initial tensile orientation <001> [135] and (b) in a polycrystalline Fe-30Mn-6Al austenitic alloy [136]. Alloy compositions are given in weight %. “Reproduced with permission from *Scripta Mater.*, 63, 1189 (2010). Copyright 2010 Elsevier.”

Fig. 19a and b [45]. As a result, despite the occurrence of a considerable amount of hydrogen-assisted damage, the hydrogen embrittlement susceptibility of an Fe-32Mn alloy is lower than that of Fe-Mn-C TWIP steels and other binary Fe-Mn alloys as shown in **Fig. 19c**.

Furthermore, ϵ -martensite has a certain robustness against fatigue crack growth under hydrogen environment. It has been reported that the diffusivity of hydrogen is a primary factor affecting fatigue crack growth resistance under hydrogen environment. Thus, α' -martensite that offers faster diffusivity for hydrogen compared to its diffusivity in austenite plays a critical role in accelerating the fatigue crack growth in a hydrogen atmosphere. An example of type 304 metastable austenitic steel is shown in **Fig. 20**. In contrast, ϵ -martensite is considered to show hydrogen diffusivity similar to that in austenite, because ϵ -martensite also has a closed-packed lattice structure. This low diffusivity of hydrogen in ϵ -martensite renders a high-Mn austenitic steel fatigue-resistant in hydrogen environment as shown in **Fig. 20**.

In the previous paragraphs, we introduced methods for the suppression of negative hydrogen effects on ductility. However, hydrogen can have a positive effect too as it has been shown to actually enhance ductility under certain optimal conditions. For example hydrogen has been reported to decrease the stacking fault energy of austenite [129–132], leading to deformation twinning [132–134] in austenitic steels. Some high-Mn austenitic steels also show hydrogen-enhanced deformation twinning [135,136]. The enhanced twinning leads to a high work hardening capacity, improving uniform elongation in case the twinning does not cause twin and grain boundary cracking, as shown in **Fig. 21**. A successful example of the positive effect of hydrogen was first reported in a single-crystalline Hadfield steel (**Fig. 21a**) [135]. After that, a polycrystalline high-Mn austenitic steel was also found to show an improvement in elongation by hydrogen charging (**Fig. 21b**) [136]. Such positive utilization of solute hydrogen can be expected to be studied and exploited more extensively in future austenitic alloy concepts.

Summary

In this review, we introduced the microstructural and compositional factors affecting the hydrogen embrittlement susceptibility of high-Mn austenitic steels. The primary factors contributing to the embrittlement are stacking fault energy, austenite phase stability, and associated hydrogen segregation on the phase, grain, and twin boundaries. These factors affect micro-stress concentrations and the local diffusible hydrogen content, which acts on the HELP effect, on hydrogen-enhanced decohesion, as well as on hydrogen-enhanced strain-induced vacancy formation. Although high-Mn austenitic steels are more susceptible to hydrogen embrittlement compared to stable austenitic stainless steels, various methods to improve the resistance to hydrogen embrittlement have been reported, such as Al addition, grain refinement, and positive utilization of ductile ϵ -martensite. Better understanding of the various hydrogen embrittlement mechanisms and their interactions in high-Mn austenitic steels would help in expanding the range of applications of

these steels as a new class of hydrogen-resistant high-strength materials.

Acknowledgements

M. Koyama and K. Tsuzaki acknowledge the financial support by KAKENHI (15K18235 and 16H06365) and the Japan Science and Technology Agency (grant number: 20100113) under Industry-Academia Collaborative R&D Program “Heterogeneous Structure Control: Towards Innovative Development of Metallic Structural Materials”.

REFERENCES

- [1] Hadfield RA. Manganese-steel: I. Manganese in its application to metallurgy: II. Some newly-discovered properties of iron and manganese. Institution. 1888.
- [2] Grässel O, Krüger L, Frommeyer G, Meyer LW. High strength Fe–Mn–(Al, Si) TRIP/TWIP steels development – properties – application. *Int J Plasticity* 2000;16:1391–409.
- [3] Koyama M, Sawaguchi T, Lee T, Lee CS, Tsuzaki K. Work hardening associated with ϵ -martensitic transformation, deformation twinning and dynamic strain aging in Fe–17Mn–0.6 C and Fe–17Mn–0.8 C TWIP steels. *Mater Sci Eng A* 2011;528:7310–6.
- [4] Bouaziz O, Allain S, Scott CP, Cugy P, Barbier D. High manganese austenitic twinning induced plasticity steels: a review of the microstructure properties relationships. *Curr Opin Solid State Mater Sci* 2011;15:141–68.
- [5] Steinmetz DR, Jäpel T, Wietbrock B, Eisenlohr P, Gutierrez-Urrutia I, Saeed–Akbari A, et al. Revealing the strain-hardening behavior of twinning-induced plasticity steels: theory, simulations, experiments. *Acta Mater* 2013;61:494–510.
- [6] Raabe D, Springer H, Gutierrez-Urrutia I, Roters F, Bausch M, Seol J-B, et al. Alloy design, combinatorial synthesis, and microstructure–property relations for low-density Fe–Mn–Al–C austenitic steels. *JOM* 2014;66:1845–56.
- [7] Sawaguchi T, Bujoreanu L-G, Kikuchi T, Ogawa K, Koyama M, Murakami M. Mechanism of reversible transformation-induced plasticity of Fe–Mn–Si shape memory alloys. *Scr Mater* 2008;59:826–9.
- [8] Ju Y-B, Koyama M, Sawaguchi T, Tsuzaki K, Noguchi H. In situ microscopic observations of low-cycle fatigue-crack propagation in high-Mn austenitic alloys with deformation-induced ϵ -martensitic transformation. *Acta Mater* 2016;112:326–36.
- [9] Sawaguchi T, Maruyama T, Otsuka H, Kushibe A, Inoue Y, Tsuzaki K. Design concept and applications of Fe–Mn–Si-based alloys – from shape-memory to seismic response control. *Mater Trans* 2016;57:283–93.
- [10] Schinhammer M, Häni AC, Löffler JF, Uggowitzer PJ. Design strategy for biodegradable Fe-based alloys for medical applications. *Acta Biomater* 2010;6:1705–13.
- [11] Schinhammer M, Pecnik CM, Rechberger F, Häni AC, Löffler JF, Uggowitzer PJ. Recrystallization behavior, microstructure evolution and mechanical properties of biodegradable Fe–Mn–C(–Pd) TWIP alloys. *Acta Mater* 2012;60:2746–56.
- [12] Heiden M, Walker E, Nauman E, Stanciu L. Evolution of novel bioresorbable iron–manganese implant surfaces and their degradation behaviors in vitro. *J Biomed Mater Res Part A* 2015;103:185–93.

- [13] Gludovatz B, Hohenwarter A, Catoor D, Chang EH, George EP, Ritchie RO. A fracture-resistant high-entropy alloy for cryogenic applications. *Science* 2014;345:1153–8.
- [14] Li Z, Pradeep KG, Deng Y, Raabe D, Tasan CC. Metastable high-entropy dual-phase alloys overcome the strength-ductility trade-off. *Nature* 2016;534:227–30.
- [15] Raabe D, Tasan CC, Springer H, Bausch M. From high-entropy alloys to high-entropy steels. *Steel Res Int* 2015;86:1127–38.
- [16] Ueji R, Kondo D, Takagi Y, Mizuguchi T, Tanaka Y, Shinagawa K. Grain size effect on high-speed deformation of Hadfield steel. *J Mater Sci* 2012;47:7946–53.
- [17] Curtze S, Kuokkala VT. Dependence of tensile deformation behavior of TWIP steels on stacking fault energy, temperature and strain rate. *Acta Mater* 2010;58:5129–41.
- [18] Sasaki T, Watanabe K, Nohara K, Ono Y, Kondo N, Sato S. Physical and mechanical properties of high manganese non-magnetic steel and its application to various products for commercial use. *Trans Iron Steel Inst Jpn* 1982;22:1010–20.
- [19] Koyama M, Lee T, Lee CS, Tsuzaki K. Grain refinement effect on cryogenic tensile ductility in a Fe–Mn–C twinning-induced plasticity steel. *Mater Des* 2013;49:234–41.
- [20] So KH, Kim JS, Chun YS, Park K-T, Lee Y-K, Lee CS. Hydrogen delayed fracture properties and internal hydrogen behavior of a Fe-18Mn-1.5Al-0.6C TWIP steel. *ISIJ Int* 2009;49:1952–9.
- [21] Ronevich JA, Speer JG, Matlock DK. Hydrogen embrittlement of commercially produced advanced high strength sheet steels. *SAE Int J Mater Manuf* 2010;3:255–67.
- [22] Chun YS, Lee J, Bae CM, Park K-T, Lee CS. Caliber-rolled TWIP steel for high-strength wire rods with enhanced hydrogen-delayed fracture resistance. *Scr Mater* 2012;67:681–4.
- [23] Mittal SC, Prasad RC, Deshmukh MB. Effect of hydrogen on fracture of austenitic Fe-Mn-Al steel. *ISIJ Int* 1994;34:211–6.
- [24] Koyama M, Akiyama E, Tsuzaki K. Hydrogen embrittlement in a Fe–Mn–C ternary twinning-induced plasticity steel. *Corros Sci* 2012;54:1–4.
- [25] Chin K-G, Kang C-Y, Shin SY, Hong S, Lee S, Kim HS, et al. Effects of Al addition on deformation and fracture mechanisms in two high manganese TWIP steels. *Mater Sci Eng A* 2011;528:2922–8.
- [26] De Cooman BC, Kim J, Chin K-G. High Mn TWIP steels for automotive applications. INTECH Open Access Publisher; 2011. Available from: <http://www.intechopen.com/books/new-trends-and-developments-in-automotive-system-engineering/high-mn-twip-steels-for-automotive-applications>.
- [27] Hong S, Shin SY, Kim HS, Lee S, Kim S-K, Chin K-G, et al. Effects of inclusions on delayed fracture properties of three twinning induced plasticity (TWIP) steels. *Metall Mater Trans A* 2013;44:776–86.
- [28] van Tol RT, Zhao L, Bracke L, Kömmelt P, Sietsma J. Investigation of the delayed fracture phenomenon in deep-drawn austenitic manganese-based twinning-induced plasticity steels. *Metall Mater Trans A* 2013;44:4654–60.
- [29] Martin M, Weber S, Theisen W, Michler T, Naumann J. Effect of alloying elements on hydrogen environment embrittlement of AISI type 304 austenitic stainless steel. *Int J Hydrogen Energy* 2011;36:15888–98.
- [30] Michler T, San Marchi C, Naumann J, Weber S, Martin M. Hydrogen environment embrittlement of stable austenitic steels. *Int J Hydrogen Energy* 2012;37:16231–46.
- [31] Ronevich JA, Kim SK, Speer JG, Matlock DK. Hydrogen effects on cathodically charged twinning-induced plasticity steel. *Scr Mater* 2012;66:956–9.
- [32] Chun YS, Park K-T, Lee CS. Delayed static failure of twinning-induced plasticity steels. *Scr Mater* 2012;66:960–5.
- [33] Koyama M, Akiyama E, Tsuzaki K. Hydrogen embrittlement in Al-added twinning-induced plasticity steels evaluated by tensile tests during hydrogen charging. *ISIJ Int* 2012;52:2283–7.
- [34] Troiano AR. The role of hydrogen and other interstitials in the mechanical behavior of metals. *Trans ASM* 1960;52:54–80.
- [35] Wang M, Akiyama E, Tsuzaki K. Hydrogen degradation of a boron-bearing steel with 1050 and 1300 MPa strength levels. *Scr Mater* 2005;52:403–8.
- [36] Toribio J, Kharin V, Lorenzo M, Vergara D. Role of drawing-induced residual stresses and strains in the hydrogen embrittlement susceptibility of prestressing steels. *Corros Sci* 2011;53:3346–55.
- [37] Enos DG, Scully JR. A critical-strain criterion for hydrogen embrittlement of cold-drawn, ultrafine pearlitic steel. *Metall Mater Trans A* 2002;33:1151–66.
- [38] Wang M, Akiyama E, Tsuzaki K. Effect of hydrogen on the fracture behavior of high strength steel during slow strain rate test. *Corros Sci* 2007;49:4081–97.
- [39] Takagi S, Toji Y, Yoshino M, Hasegawa K. Hydrogen embrittlement resistance evaluation of ultra high strength steel sheets for automobiles. *ISIJ Int* 2012;52:316–22.
- [40] Barnoush A, Vehoff H. Recent developments in the study of hydrogen embrittlement: hydrogen effect on dislocation nucleation. *Acta Mater* 2010;58:5274–85.
- [41] Eliezer D, Chakrapani DG, Altstetter CJ, Pugh EN. The influence of austenite stability on the hydrogen embrittlement and stress-corrosion cracking of stainless steel. *Metall Trans A* 1979;10:935–41.
- [42] Zhang L, Wen M, Imade M, Fukuyama S, Yokogawa K. Effect of nickel equivalent on hydrogen gas embrittlement of austenitic stainless steels based on type 316 at low temperatures. *Acta Mater* 2008;56:3414–21.
- [43] Dieudonné T, Marchetti L, Wery M, Chêne J, Allely C, Cugy P, et al. Role of copper and aluminum additions on the hydrogen embrittlement susceptibility of austenitic Fe–Mn–C TWIP steels. *Corros Sci* 2014;82:218–26.
- [44] Koyama M, Akiyama E, Tsuzaki K. Hydrogen-induced delayed fracture of a Fe–22Mn–0.6 C steel pre-strained at different strain rates. *Scr Mater* 2012;66:947–50.
- [45] Koyama M, Okazaki S, Sawaguchi T, Tsuzaki K. Hydrogen embrittlement susceptibility of Fe-Mn binary alloys with high Mn content: effects of stable and metastable ε-martensite, and Mn concentration. *Metall Mater Trans A* 2016;47:2656–73.
- [46] Kim Y, Kang N, Park Y, Choi I, Kim G, Kim S, et al. Effects of the strain induced martensite transformation on the delayed fracture for Al-added TWIP steel. *J Korean Inst Metals Mater* 2008;46:780–7.
- [47] Venables JA. The martensite transformation in stainless steel. *Philos Mag* 1962;7:35–44.
- [48] Olson GB, Cohen M. A mechanism for the strain-induced nucleation of martensitic transformations. *J Less Common Metals* 1972;28:107–18.
- [49] Tomota Y, Strum M, Morris JW. Microstructural dependence of Fe-high Mn tensile behavior. *Metall Trans A* 1986;17:537–47.
- [50] Wong SL, Madivala M, Prahl U, Roters F, Raabe D. A crystal plasticity model for twinning- and transformation-induced plasticity. *Acta Mater* 2016;118:140–51.
- [51] Remy L, Pineau A. Twinning and strain-induced F.C.C. → H.C.P. transformation in the Fe-Mn-Cr-C system. *Mater Sci Eng* 1977;28:99–107.

- [52] Takaki S, Furuya T, Tokunaga Y. Effect of Si and Al additions on the low temperature toughness and fracture mode of Fe–27Mn alloys. *ISIJ Int* 1990;30:632–8.
- [53] Koyama M, Sawaguchi T, Tsuzaki K. Quasi-cleavage fracture along annealing twin boundaries in a Fe–Mn–C austenitic steel. *ISIJ Int* 2012;52:161–3.
- [54] Koyama M, Sawaguchi T, Tsuzaki K. Premature fracture mechanism in an Fe–Mn–C austenitic steel. *Metall Mater Trans A* 2012;43:4063–74.
- [55] Koyama M, Sawaguchi T, Tsuzaki K. Effects of Si on tensile properties associated with deformation-induced ϵ -martensitic transformation in high Mn austenitic alloys. *Mater Trans* 2015;56:819–25.
- [56] Chun YS, Kim JS, Park K-T, Lee Y-K, Lee CS. Role of ϵ martensite in tensile properties and hydrogen degradation of high-Mn steels. *Mater Sci Eng A* 2012;533:87–95.
- [57] Gutierrez-Urrutia I, Raabe D. High strength and ductile low density austenitic FeMnAlC steels: simplex and alloys strengthened by nanoscale ordered carbides. *Mater Sci Technol* 2014;30:1099–104.
- [58] Yao MJ, Dey P, Seol JB, Choi P, Herbig M, Marceau RKW, et al. Combined atom probe tomography and density functional theory investigation of the Al off-stoichiometry of κ -carbides in an austenitic Fe–Mn–Al–C low density steel. *Acta Mater* 2016;106:229–38.
- [59] Choi K, Seo C-H, Lee H, Kim SK, Kwak JH, Chin KG, et al. Effect of aging on the microstructure and deformation behavior of austenite base lightweight Fe–28Mn–9Al–0.8C steel. *Scr Mater* 2010;63:1028–31.
- [60] Gutierrez-Urrutia I, Raabe D. Influence of Al content and precipitation state on the mechanical behavior of austenitic high-Mn low-density steels. *Scr Mater* 2013;68:343–7.
- [61] Welsch E, Ponge D, Hafez Haghigat SM, Sandlöbes S, Choi P, Herbig M, et al. Strain hardening by dynamic slip band refinement in a high-Mn lightweight steel. *Acta Mater* 2016;116:188–99.
- [62] Calcagnotto M, Ponge D, Demir E, Raabe D. Orientation gradients and geometrically necessary dislocations in ultrafine grained dual-phase steels studied by 2D and 3D EBSD. *Mater Sci Eng A* 2010;527:2738–46.
- [63] Gutierrez-Urrutia I, Zaefferer S, Raabe D. Electron channeling contrast imaging of twins and dislocations in twinning-induced plasticity steels under controlled diffraction conditions in a scanning electron microscope. *Scr Mater* 2009;61:737–40.
- [64] Zaefferer S, Elhami N-N. Theory and application of electron channelling contrast imaging under controlled diffraction conditions. *Acta Mater* 2014;75:20–50.
- [65] Michler T. Hydrogen environment embrittlement. MPIE work shop on hydrogen embrittlement in steels 2013, available from: http://www.mpie.de/uploads/media/HES_Workshop_Michler.pdf.
- [66] Sofronis P, Liang Y, Aravas N. Hydrogen induced shear localization of the plastic flow in metals and alloys. *Eur J Mech A/Solids* 2001;20:857–72.
- [67] von Pezold J, Lymerakis L, Neugebeauer J. Hydrogen-enhanced local plasticity at dilute bulk H concentrations: the role of H–H interactions and the formation of local hydrides. *Acta Mater* 2011;59:2969–80.
- [68] Robertson IM, Sofronis P, Nagao A, Martin ML, Wang S, Gross DW, et al. Hydrogen embrittlement understood. *Metall Mater Trans B* 2015;46:1085–103.
- [69] Nagumo M. Function of hydrogen in embrittlement of high-strength steels. *ISIJ Int* 2001;41:590–8.
- [70] Nagumo M. Hydrogen related failure of steels – a new aspect. *Mater Sci Technol* 2004;20:940–50.
- [71] Ahn DC, Sofronis P, Dodds Jr RH. On hydrogen-induced plastic flow localization during void growth and coalescence. *Int J Hydrogen Energy* 2007;32:3734–42.
- [72] Koyama M, Springer H, Merzlikin SV, Tsuzaki K, Akiyama E, Raabe D. Hydrogen embrittlement associated with strain localization in a precipitation-hardened Fe–Mn–Al–C light weight austenitic steel. *Int J Hydrogen Energy* 2014;39:4634–46.
- [73] Koyama M, Akiyama E, Sawaguchi T, Raabe D, Tsuzaki K. Hydrogen-induced cracking at grain and twin boundaries in an Fe–Mn–C austenitic steel. *Scr Mater* 2012;66:459–62.
- [74] Koyama M, Akiyama E, Sawaguchi T, Ogawa K, Kireeva IV, Chumlyakov YI, et al. Hydrogen-assisted quasi-cleavage fracture in a single crystalline type 316 austenitic stainless steel. *Corros Sci* 2013;75:345–53.
- [75] Koyama M, Akiyama E, Tsuzaki K, Raabe D. Hydrogen-assisted failure in a twinning-induced plasticity steel studied under in situ hydrogen charging by electron channeling contrast imaging. *Acta Mater* 2013;61:4607–18.
- [76] Ryu JH, Kim SK, Lee CS, Suh D-W, Bhadeshia HKDH. Effect of aluminium on hydrogen-induced fracture behaviour in austenitic Fe–Mn–C steel. *Proc R Soc A Math Phys Eng Sci* 2013;469.
- [77] Michler T, Naumann J. Hydrogen embrittlement of Cr–Mn–N-austenitic stainless steels. *Int J Hydrogen Energy* 2010;35:1485–92.
- [78] Müllner P, Solenthaler C, Uggowitzer PJ, Speidel MO. Brittle fracture in austenitic steel. *Acta Metall Mater* 1994;42:2211–7.
- [79] Müllner P. On the ductile to brittle transition in austenitic steel. *Mater Sci Eng A* 1997;234:94–7.
- [80] Christian JW, Mahajan S. Deformation twinning. *Prog Mater Sci* 1995;39:1–157.
- [81] Ng BC, Simkin BA, Crimp MA, Bieler TR. The role of mechanical twinning on microcrack nucleation and crack propagation in a near- γ TiAl alloy. *Intermetallics* 2004;12:1317–23.
- [82] Koyama M, Bashir A, Rohwerder M, Merzlikin SV, Akiyama E, Tsuzaki K, et al. Spatially and kinetically resolved mapping of hydrogen in a twinning-induced plasticity steel by use of scanning Kelvin probe force microscopy. *J Electrochem Soc* 2015;162:C638–47.
- [83] Saito H, Miyazawa KI, Ishida Y. Tritium transmission electron microscopic autoradiography of hydrogen trapping sites at interfaces in an austenitic stainless steel SUS316L. *Nippon Kinzoku Gakkaishi J Jpn Inst Metals* 1991;55:366–75.
- [84] Saito H, Mori M, Ishida Y. Observation of hydrogen trapping sites at 77 K exposure in SUS316L steel by means of tritium TEM autoradiography. *Nippon Kinzoku Gakkai-Shi* 1995;59:910–6.
- [85] Mahajan S, Chin GY. Twin-slip, twin-twin and slip-twin interactions in Co-8 wt.% Fe alloy single crystals. *Acta Metall* 1973;21:173–9.
- [86] Rémy L. Twin-slip interaction in f.c.c. crystals. *Acta Metall* 1977;25:711–4.
- [87] Rémy L. The interaction between slip and twinning systems and the influence of twinning on the mechanical behavior of fcc metals and alloys. *Metall Trans A* 1981;12:387–408.
- [88] Wang YB, Sui ML. Atomic-scale in situ observation of lattice dislocations passing through twin boundaries. *Appl Phys Lett* 2009;94:021909.
- [89] Ferreira PJ, Robertson IM, Birnbaum HK. Hydrogen effects on the interaction between dislocations. *Acta Mater* 1998;46:1749–57.
- [90] Bal B, Koyama M, Gerstein G, Maier HJ, Tsuzaki K. Effect of strain rate on hydrogen embrittlement susceptibility of twinning-induced plasticity steel pre-charged with

- high-pressure hydrogen gas. *Int J Hydrogen Energy* 2016;41:15362–72.
- [91] Du YA, Ismer L, Rogal J, Hickel T, Neugebauer J, Drautz R. First-principles study on the interaction of H interstitials with grain boundaries in α - and γ -Fe. *Phys Rev B* 2011;84:144121.
- [92] Evers S, Rohwerder M. The hydrogen electrode in the “dry”: a Kelvin probe approach to measuring hydrogen in metals. *Electrochim Commun* 2012;24:85–8.
- [93] Tien J, Thompson AW, Bernstein IM, Richards RJ. Hydrogen transport by dislocations. *Metall Trans A* 1976;7:821–9.
- [94] Frankel GS, Latanision RM. Hydrogen transport during deformation in nickel: part II. Single crystal nickel. *Metall Trans A* 1986;17:869–75.
- [95] Dadfarnia M, Martin ML, Nagao A, Sofronis P, Robertson IM. Modeling hydrogen transport by dislocations. *J Mech Phys Solids* 2015;78:511–25.
- [96] Koyama M, Akiyama E, Tsuzaki K. Effects of static and dynamic strain aging on hydrogen embrittlement in TWIP steels containing Al. *ISIJ Int* 2013;53:1268–74.
- [97] Chen L, Kim H-S, Kim S-K, De Cooman BC. Localized deformation due to portevin-LeChatelier effect in 18Mn-0.6C TWIP austenitic steel. *ISIJ Int* 2007;47:1804–12.
- [98] Canadinc D, Efsthathiou C, Sehitoglu H. On the negative strain rate sensitivity of Hadfield steel. *Scr Mater* 2008;59:1103–6.
- [99] Dastur Y, Leslie W. Mechanism of work hardening in Hadfield manganese steel. *Metall Trans A* 1981;12:749–59.
- [100] Lee S-J, Kim J, Kane SN, Cooman BCD. On the origin of dynamic strain aging in twinning-induced plasticity steels. *Acta Mater* 2011;59:6809–19.
- [101] Allain S, Bouaziz O, Lebedkina T, Lebyodkin M. Relationship between relaxation mechanisms and strain aging in an austenitic FeMnC steel. *Scr Mater* 2011;64:741–4.
- [102] Koyama M, Akiyama E, Tsuzaki K. Factors affecting static strain aging under stress at room temperature in a Fe–Mn–C twinning-induced plasticity steel. *ISIJ Int* 2013;53:1089–96.
- [103] Koyama M, Akiyama E, Tsuzaki K. Effect of hydrogen content on the embrittlement in a Fe–Mn–C twinning-induced plasticity steel. *Corros Sci* 2012;59:277–81.
- [104] Malard B, Remy B, Scott C, Deschamps A, Chêne J, Dieudonné T, et al. Hydrogen trapping by VC precipitates and structural defects in a high strength Fe–Mn–C steel studied by small-angle neutron scattering. *Mater Sci Eng A* 2012;536:110–6.
- [105] Park I-J, Jo SY, Kang M, Lee S-M, Lee Y-K. The effect of Ti precipitates on hydrogen embrittlement of Fe–18Mn–0.6C–2Al–xTi twinning-induced plasticity steel. *Corros Sci* 2014;89:38–45.
- [106] Suh D-W. Critical assessment 2: hydrogen induced fracture in austenitic, high-manganese TWIP steel. *Mater Sci Technol* 2014;30:1131–4.
- [107] Song EJ, Bhadeshia HKDH, Suh D-W. Interaction of aluminium with hydrogen in twinning-induced plasticity steel. *Scr Mater* 2014;87:9–12.
- [108] Han DK, Lee SK, Noh SJ, Kim SK, Suh DW. Effect of aluminium on hydrogen permeation of high-manganese twinning-induced plasticity steel. *Scr Mater* 2015;99:45–8.
- [109] Park I-J, Jeong K-H, Jung J-G, Lee CS, Lee Y-K. The mechanism of enhanced resistance to the hydrogen delayed fracture in Al-added Fe–18Mn–0.6C twinning-induced plasticity steels. *Int J Hydrogen Energy* 2012;37:9925–32.
- [110] Chen FC, Chou CP, Li P, Chu SL. Effect of aluminium on TRIP Fe–Mn–Al alloy steels at room temperature. *Mater Sci Eng A* 1993;160:261–70.
- [111] Park K-T, Jin KG, Han SH, Hwang SW, Choi K, Lee CS. Stacking fault energy and plastic deformation of fully austenitic high manganese steels: effect of Al addition. *Mater Sci Eng A* 2010;527:3651–61.
- [112] Jin JE, Lee YK. Effects of Al on microstructure and tensile properties of C-bearing high Mn TWIP steel. *Acta Mater* 2012;60:1680–8.
- [113] Shun T, Wan CM, Byrne JG. A study of work hardening in austenitic Fe–Mn–C and Fe–Mn–Al–C alloys. *Acta Metall Mater* 1992;40:3407–12.
- [114] Han DK, Kim YM, Han HN, Bhadeshia HKDH, Suh D-W. Hydrogen and aluminium in high-manganese twinning-induced plasticity steel. *Scr Mater* 2014;80:9–12.
- [115] Lee S-M, Park I-J, Jung J-G, Lee Y-K. The effect of Si on hydrogen embrittlement of Fe–18Mn–0.6C–xSi twinning-induced plasticity steels. *Acta Mater* 2016;103:264–72.
- [116] Raabe D, Herbig M, Sandlöbes S, Li Y, Tytko D, Kuzmina M, et al. Grain boundary segregation engineering in metallic alloys: a pathway to the design of interfaces. *Curr Opin Solid State Mater Sci* 2014;18:253–61.
- [117] Kuzmina M, Ponge D, Raabe D. Grain boundary segregation engineering and austenite reversion turn embrittlement into toughness: example of a 9 wt.% medium Mn steel. *Acta Mater* 2015;86:182–92.
- [118] Michler T, Berreth K, Naumann J, Sattler E. Analysis of martensitic transformation in 304 type stainless steels tensile tested in high pressure hydrogen atmosphere by means of XRD and magnetic induction. *Int J Hydrogen Energy* 2012;37:3567–72.
- [119] Zan N, Ding H, Guo X, Tang Z, Bleck W. Effects of grain size on hydrogen embrittlement in a Fe–22Mn–0.6C TWIP steel. *Int J Hydrogen Energy* 2015;40:10687–96.
- [120] Park I-J, Lee S, Jeon H, Lee Y-K. The advantage of grain refinement in the hydrogen embrittlement of Fe–18Mn–0.6C twinning-induced plasticity steel. *Corros Sci* 2015;93:63–9.
- [121] Bai Y, Momotani Y, Chen MC, Shibata A, Tsuji N. Effect of grain refinement on hydrogen embrittlement behaviors of high-Mn TWIP steel. *Mater Sci Eng A* 2016;651:935–44.
- [122] Jeon H-H, Lee S-M, Han J, Park I-J, Lee Y-K. The effect of Zn coating layers on the hydrogen embrittlement of hot-dip galvanized twinning-induced plasticity steel. *Corros Sci* 2016;111:267–74.
- [123] Tsuzaki K, Fukuda K, Koyama M, Matsunaga H. Hexagonal close-packed martensite-related fatigue crack growth under the influence of hydrogen: example of Fe–15Mn–10Cr–8Ni–4Si austenitic alloy. *Scr Mater* 2016;113:6–9.
- [124] Gutierrez-Urrutia I, Raabe D. Grain size effect on strain hardening in twinning-induced plasticity steels. *Scr Mater* 2012;66:992–6.
- [125] Beal C, Kleber X, Fabregue D, Bouzekri M. Liquid zinc embrittlement of twinning-induced plasticity steel. *Scr Mater* 2012;66:1030–3.
- [126] Beal C, Kleber X, Fabregue D, Bouzekri M. Embrittlement of a zinc coated high manganese TWIP steel. *Mater Sci Eng A* 2012;543:76–83.
- [127] Koyama M, Tasan CC, Akiyama E, Tsuzaki K, Raabe D. Hydrogen-assisted decohesion and localized plasticity in dual-phase steel. *Acta Mater* 2014;70:174–87.
- [128] Koyama M, Tasan CC, Nagashima T, Akiyama E, Raabe D, Tsuzaki K. Hydrogen-assisted damage in austenite/martensite dual-phase steel. *Philos Mag Lett* 2016;96:9–18.
- [129] Whiteman MB, Troiano AR. The influence of hydrogen on the stacking fault energy of an austenitic stainless steel. *Phys Status Solidi (b)* 1964;7:K109–10.

- [130] Ferreira P, Robertson IM, Birnbaum H. Influence of hydrogen on the stacking-fault energy of an austenitic stainless steel. *Mater Sci Forum Trans Tech Publ* 1996;93–6.
- [131] Pontini AE, Hermida JD. X-ray diffraction measurement of the stacking fault energy reduction induced by hydrogen in an AISI 304 steel. *Scr Mater* 1997;37:1831–7.
- [132] Kireeva IV, Chumlyakov YI, Tverskov AV, Maier H. Effect of hydrogen on orientation dependence of critical shear stress and mechanism of straining in single crystals of stable stainless steel. *Tech Phys Lett* 2011;37:522–5.
- [133] Rigsbee JM, Benson RB. A TEM investigation of hydrogen-induced deformation twinning and associated martensitic phases in 304-type stainless steel. *J Mater Sci* 1977;12:406–9.
- [134] Sato K, Ichinose M, Hirotsu Y, Inoue Y. Effects of deformation induced phase transformation and twinning on the mechanical properties of austenitic Fe-Mn-Al alloys. *ISIJ Int* 1989;29:868–77.
- [135] Astafurova EG, Zakharova GG, Maier HJ. Hydrogen-induced twinning in $\langle 0\ 0\ 1 \rangle$ Hadfield steel single crystals. *Scr Mater* 2010;63:1189–92.
- [136] Yamada K, Koyama M, Kaneko T, Tsuzaki K. Positive and negative effects of hydrogen on tensile behavior in polycrystalline Fe–30Mn–(6–x) Si–xAl austenitic alloys. *Scr Mater* 2015;105:54–7.